Journal Pre-proofs

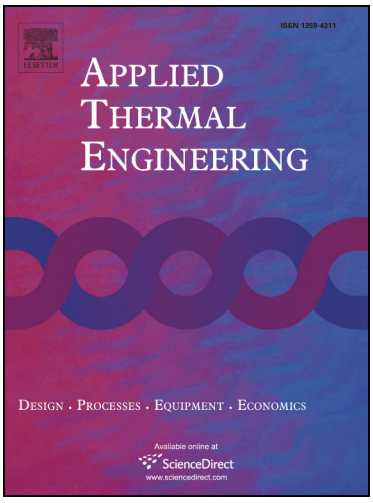


Research Paper

# Experimental and numerical study on the heat transfer performance of the radiant floor heating condenser with composite phase change material

Tingting Jiang, Chenxiao Zheng, Shijun You, Huan Zhang, Zhenjing Wu, Yaran Wang, Shen Wei

PII: S1359-4311(22)00692-5
DOI: https://doi.org/10.1016/j.applthermaleng.2022.118749
Reference: ATE 118749

To appear in: *Applied Thermal Engineering*

Received Date: 10 November 2021
Revised Date: 20 April 2022
Accepted Date: 27 May 2022

Please cite this article as: T. Jiang, C. Zheng, S. You, H. Zhang, Z. Wu, Y. Wang, S. Wei, Experimental and numerical study on the heat transfer performance of the radiant floor heating condenser with composite phase change material, *Applied Thermal Engineering* (2022), doi: https://doi.org/10.1016/j.applthermaleng.2022.118749

This is a PDF file of an article that has undergone enhancements after acceptance, such as the addition of a cover page and metadata, and formatting for readability, but it is not yet the definitive version of record. This version will undergo additional copyediting, typesetting and review before it is published in its final form, but we are providing this version to give early visibility of the article. Please note that, during the production process, errors may be discovered which could affect the content, and all legal disclaimers that apply to the journal pertain.

© 2022 Published by Elsevier Ltd.

Journal Pre-proofs

# Experimental and numerical study on the heat transfer performance of the radiant floor heating condenser with composite phase change material

Tingting Jiang [a, 1], Chenxiao Zheng [b, 1], Shijun You [a, c], Huan Zhang [a, c], Zhenjing Wu [d], Yaran Wang [a, c*], Shen Wei [e]

[a] School of Environmental Science and Engineering, Tianjin University, Jinnan District, Tianjin 300350, PR China

[b] School of Mechanical Engineering, Tianjin University of Commerce, Beichen District, Tianjin 300134, PR China

[c] Key Laboratory of Efficient Utilization of Low and Medium Grade Energy (Tianjin University), Ministry of Education of China, Tianjin 300350, PR China.

[d] School of Energy and Safety Engineering, Tianjin Chengjian University, Xiqing District, Tianjin 300384, PR China

[e] The Bartlett School of Construction and Project Management, University College London (UCL), 1-19 Torrington Place, London WC1E 7HB, United Kingdom.

Journal Pre-proofs

## Abstract

Traditional hot-water ASHP systems have disadvantage of low energy efficiency due to the requirement of secondary heat exchange. To maintain the stability of indoor air temperature during defrosting, the existing ASHP systems adopt heat exchanger to

* Corresponding author. Tel.: +8602227892626; fax: +8602227892626.

*E-mail addresses:* yaran_wang@tju.edu.cn

store heat, which increases the system complexity. To overcome these obstacles, a novel ASHP system integrated with radiant floor heating condenser (RFHC) is proposed, which uses refrigerant as working fluid to exchange heat with indoor environment directly. In addition, the composite phase change material (CPCM) is added in the RFHC for heat storage. Experiments are conducted and results show that compared with traditional ASHP systems, the proposed system has higher energy efficiency and can reduce indoor air temperature fluctuation under defrosting condition. A detailed numerical model of the RFHC is established and validated with the experimental data, and then the impacts of the operating and structural parameters on the heat transfer performance of the RFHC system are investigated. Results show that under the indoor air temperature of test room keeps at 18.0 °C, the optimal operating condition of this system is the condensing temperature with 38.0 °C and the refrigerant mass flow rate with 3.8 kg· h$^{-1}$. The optimal structural scheme of the RFHC is the copper pipe spacing with 0.25 m and the length of copper pipe with 12.0 m.

**Keywords**: radiant floor heating condenser; composite phase change material; numerical model; heat transfer performance; structural scheme

**Nomenclature**

| | | | |
|---|---|---|---|
| $A$ | area (m$^2$) | $\theta$ | excess temperature (°C) |
| $a$ | thermal diffusivity (m$^2$· s$^{-1}$) | $\rho$ | molecular density (kg· m$^{-3}$) |
| $C$ | correlation coefficient | $\tau$ | time (s) |
| $c_p$ | specific heat (J· kg$^{-1}$· K$^{-1}$) | $\alpha$ | convective heat transfer coefficient (W· m$^{-2}$· K$^{-1}$) |
| $D$ | inner diameter (m) | $\mu$ | dynamic viscosity (Pa· s) |
| $D_w$ | outer diameter (m) | $\delta$ | thickness (m) |
| $f$ | solid fraction (%) | $\beta$ | volume expansion coefficient (1· K$^{-1}$) |
| $G$ | mass flow rate (kg· h$^{-1}$) | $\nu$ | kinematic viscosity (m$^2$· s$^{-1}$) |

Journal Pre-proofs

| | | | |
|---|---|---|---|
| $Gr$ | Grashov number | ***Subscripts*** | |
| $g$ | acceleration of gravity ($m\cdot s^{-2}$) | al | aluminum foil |
| $H$ | height (m) | c | copper pipe |
| $h$ | enthalpy ($J\cdot kg^{-1}$) | cond | condensation |
| $l$ | length (m) | conv | convective |
| $La$ | latent heating capacity (W) | d | discharge |
| $m$ | weight (kg) | e | evaporate |
| $Nu$ | Nusselt number | f | composite floor |
| $n$ | number of section | $i$ | node $i$ |
| $Pr$ | Prandtl number | in | inlet |
| $p$ | pressure (Pa) | k | condense |
| $p_c$ | critical pressure (Pa) | l | liquid phase |
| $Q$ | heating capacity (W) | m | copper pipe, aluminum foil and CPCM module package shell |
| $q$ | heat flux ($W\cdot m^{-2}$) | me | initial melting |
| $Ra$ | Rayleigh number | n | indoor air |
| $Re$ | Reynolds number | nh | non-heating |
| $Sp$ | spacing (m) | ou | outdoor air |
| $t$ | temperature ($^oC$) | out | outlet |
| $U$ | perimeter (m) | r | refrigerant |
| $u$ | flow velocity ($m\cdot s^{-1}$) | rad | radiant |
| $w$ | width (m) | s | package shell |
| $x$ | vapor quality | sat | saturation state |
| $Z_f$ | characteristic length (m) | sk | package shell without groove |
| $\Delta l$ | control volume length (m) | so | initial solidification |
| $\Delta p$ | pressure drop (Pa) | tot | total |
| **Greek symbols** | | **Abbreviations** | |
| $\lambda$ | thermal conductivity ($W\cdot m^{-1}\cdot K^{-1}$) | ASHP | air source heat pump |
| $\psi$ | flow coefficient | CPCM | composite phase change material |
| $\varepsilon$ | emissivity | RCD | reverse cycle defrosting |
| $\sigma$ | Stefan-Boltzmann constant, ($5.67\times10^{-8}\ W\cdot m^{-2}\cdot K^{-4}$) | RFHC | radiant floor heating condenser |

Journal Pre-proofs

## 1. Introduction

Building energy consumption plays an important role in global environmental issues and energy crisis [1]. In China, building energy consumption accounts for nearly 35% of the total energy usage, resulting in 30% of carbon dioxide emissions [2]. In 2020, it is announced that China will strive to reach a peak in carbon dioxide emissions by 2030 and achieve carbon neutralization by 2060 [3]. It is crucial to develop a clean energy technology with high energy efficiency.

As a mature heating technology, air source heat pump (ASHP) has been widely applied for its advantages of energy-saving, pollution-free and easy installation [4]. The common ASHP heating terminals can be categorized into hot-blast air conditioner and water-heated radiator [5]. The former employs forced-convection to exchange heat with indoor environment. The air is heated by finned coil heat exchanger and then sent into the room by fan, which can quickly adapt to dynamic heat load. Nevertheless, the sense of blowing and dryness lead to the dissatisfaction of residents, and the fan power consumption degrades the energy efficiency [6]. Besides, hot-blast air conditioner adopts the air supply mode of upper supply and bottom return, which causes the stratification of indoor vertical temperature. Fanger and Christensen [7] investigated the thermal sensation of one hundred subjects who were exposed to air velocity fluctuating in typically ventilated spaces, and results showed that the percentage of subjects dissatisfied was ascended with the increase of the air velocity and the head region was the most draught-sensitive part of the body. Gendelis et al. [8] carried out a comprehensive analysis of the thermal comfort according to the long-term monitoring data in test buildings with different ASHP systems, and suggested that the forced-

Journal Pre-proofs

convection air conditioner has poor indoor thermal comfort due to its high vertical temperature difference and air velocity. The indoor thermal comfort of the traditional air conditioner was evaluated by Shao et al. [9], and justified that the vertical temperature difference of this system was within the range of 4.1 $^{o}$C ~ 8.0 $^{o}$C, which exceeded the recommended value of 3.0 $^{o}$C in ISO 7730 standard [10]. Jin et al. [11] experimentally and numerically studied the performance of the ASHP system with an internal heat exchanger and suggested that the COP of this system was merely 1.6 ~ 2.6 when the outdoor ambient temperature varied from -26.0 $^{o}$C to 0 $^{o}$C.

With respect to the water-heated radiator, it mainly depends on radiation and natural convection for heat transfer, which has satisfied thermal comfort and small vertical temperature gradient. Causone et al. [12] conducted an experimental investigation of the floor heating system with displacement ventilation, with results showing that the indoor air could not occur the stratification phenomenon in the vertical direction. Peng et al. [13] adopted a simulation software to analyze the indoor thermal environment under different ASHP systems, and suggested that radiant heating systems were able to avoid strong draught and dry eye problem in comparison with conventional air conditioning systems. However, when the water-heated radiator is used for space heating, the heat from the refrigerant is firstly delivered to the water, and then the hot water is sent to the radiator to exchange heat with indoor environment, which degrades the energy utilization of this system. Additionally, water pump and tank, filter and other devices not only increase the system complexity, but also improve the operation and maintenance costs [14]. Xiao et al. [15] focused on the performances of the air-to-air heat pump and air-to-water heat pump through numerical simulation, and results showed that the COP of the former was superior to the latter under the ambient

temperature decreased from 7.0 °C to -20.0 °C. Congedo et al. [16] proposed an ASHP system coupled with a horizontal earth-to-air heat exchanger (EAHX) and evaluated the system performance using different coefficients, and results showed that this system had higher energy efficiency compared to traditional ASHP systems in all seasons. However, the ASHP-EAXH system still needed secondary heat exchange with water. Hu et al. [17] studied the thermal performance of different ASHP systems through experimental research, and confirmed that radiant heating systems had high operating cost.

To avoid the defects of the above heating systems, the direct radiant floor heating system has attracted a great deal of research attention, which adopts refrigerant as direct circulating medium to exchange heat with indoor environment. Compared with hot-blast air conditioner, this system is capable of creating a comfortable indoor thermal environment due to its low vertical temperature gradient and without draught sensation. Compared with water-heated radiator, this system can avoid secondary heat exchange, leading to the improvement of the energy efficiency. Wu [18] proposed a direct radiant floor heating system and evaluated its thermal performance through experimental investigation. Results showed that this system had good indoor thermal comfort since the temperature difference between human head and ankle was merely 0.4 °C. A radiant floor heating without water system was proposed by Dong et al. [19], and their analysis demonstrated that the power consumption of this system was 7.4% lower than conventional ASHP systems. Li [20] developed a numerical model to investigate the heat transfer performance of the direct condensing radiant floor heating system, and confirmed that the heat transfer coefficient of this system was 48.1% higher than that of hot-water ASHP system.

Journal Pre-proofs

Frosting is an inevitable problem when the ASHP systems operate at low ambient temperature, resulting in the depression of the system performance [21]. Besides, the indoor air temperature will fluctuate when the ASHP systems in defrosting process, which will cause the residents feel uncomfortable. To tackle these issues, the thermal energy storage technology comes to the foreground recently. Qu et al. [22] investigated the operating performance of the cascade ASHP system with a thermal energy storage based heat exchanger, and suggested that the stored thermal energy could provide for space heating during defrosting and the energy consumption was decreased by 65.1% ~ 85.2%. A comparison between a novel reverse-cycle defrosting (NRCD) method and standard reverse-cycle defrosting (SRCD) method of the multi-split ASHP system with a phase change material heat exchanger was executed by Dong et al. [23], justifying the former one made a great contribution to defrosting and heat-resumption duration. Liu et al. [24] proposed a novel PCM heat exchanger using in ASHP system, and suggested that the defrosting speed of this system was improved by 50.0% and the energy consumption was reduced by 71.0%.

However, the existing ASHP systems adopt additional heat exchanger to store heat in heating condition and release heat during defrosting, which increases the system complexity. While few scholars concentrate on the direct radiant floor heating system combined with thermal energy storage technology instead of additional heat exchanger, and the numerical simulation and optimization of this system have not been explored. In this study, a novel ASHP system coupled with RFHC and CPCM is proposed. A detailed numerical model is developed to describe the heat transfer performance of the RFHC. Experiments are carried out for the operating characteristics analysis of the RFHC system. The reliability of the numerical model of the RFHC is validated with the

experimental data. Based on the numerical model, the effects of the operating and structural parameters on the heat transfer performance of the RFHC system are investigated, and the optimal operating condition and structural scheme are obtained. The proposed system is suitable for applying in residential and commercial buildings.

## 2. Methodology

### *2.1 Physical model*

Fig. 1 shows the structure of the RFHC, which is laid with moisture-proof layer, thermal insulation layer, CPCM modules, aluminum foil, copper pipes and composite floor from bottom to top. The dry floor laying method is adopted to make the copper pipes in direct contact with the composite floor. The aluminum foil is arranged between copper pipes and composite floor to enhance the heat capacity and ensure the temperature uniformity of the composite floor surface. The copper pipes filled with R410a refrigerant are embedded in the CPCM modules, and the CPCM modules are encapsulated in the aluminum alloy plate. The CPCM modules are used to store heat under heating condition and release heat in defrosting process, which can avoid absorbing heat from indoor environment. Considering the radiant floor heating temperature and operating characteristic of the RFHC, the CPCM with phase change temperature of 26.1 $^{o}$C and the phase change latent heat of $1.81\times10^{5}$ kJ· kg$^{-1}$ is selected [25]. During the operating period, the refrigerant in copper pipes is condensed and then the heat is transferred to the CPCM modules and composite floor simultaneously via heat conduction. Then the heat from the composite floor is delivered to the indoor environment through radiation and natural convection.

Journal Pre-proofs

In order to describe the heat transfer process of the RFHC based on the numerical model, the appropriately assumptions are as follows:

(1) The flow direction of the refrigerant in copper pipes is considered as one-dimensional;

(2) The heat conduction of the copper pipes and the effect of the gravity are ignored;

(3) The solid material of each layer is evenly distributed, and the density, thermal conductivity and specific heat capacity are kept constant;

(4) All the solid materials are in close contact, regardless of contact thermal resistance;

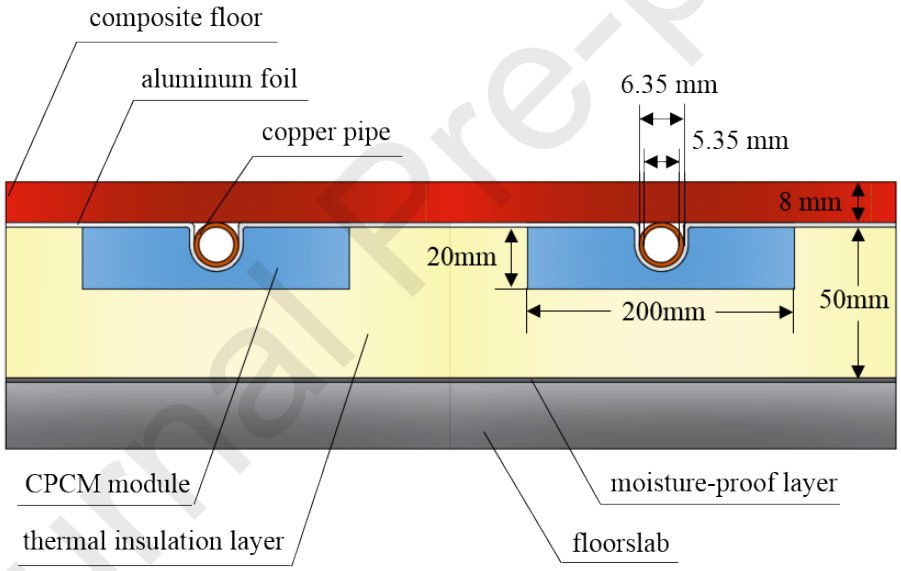


Fig. 1. The schematic of the RFHC.

*2.2 Numerical model*

The finite volume method is adopted to establish the numerical model of the RFHC. Fig. 2 shows the schematic diagram of the control volume along the refrigerant flow direction, which is divided into *n* sections. Besides, the refrigerant, copper pipe and aluminum foil as well as CPCM module package shell, CPCM module and composite

Journal Pre-proofs

floor are separated into four control volumes along the radial direction of copper pipes. Thus, there are 4 × $n$ control volumes and $\Delta l$ is the length of the control volume.

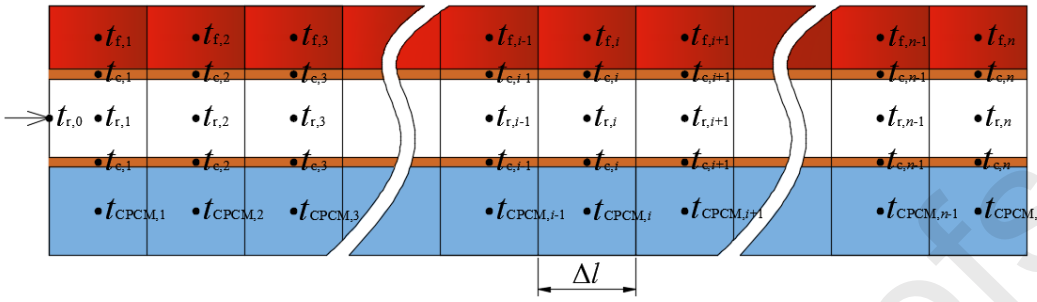


Fig. 2. Schematic diagram of control volume division of the RFHC.

2.2.1 Heat transfer of the refrigerant

The heat of the refrigerant consists of the heat change in the control volume $Q_{rc}$, heat enter the control volume due to the refrigerant flow $Q_{rf}$ and heat transfer between refrigerant and inner surface of the copper pipe $Q_{r\text{-}c}$, and their expressions can be given as:

$$Q_{rc} = Q_{rf} - Q_{r\text{-}c} \tag{1}$$

$$Q_{rc} = \frac{\pi D^2 \Delta l_i (\rho_{r,i}^{\tau} h_{r,i}^{\tau} - \rho_{r,i}^{\tau-\Delta\tau} h_{r,i}^{\tau-\Delta\tau})}{4 \cdot \Delta\tau} \tag{2}$$

$$Q_{rf} = G_r (h_{r\text{-}in,i}^{\tau} - h_{r\text{-}out,i}^{\tau}) \tag{3}$$

$$Q_{r\text{-}c} = \alpha_{r,i} A_{c,i} (t_{r,i}^{\tau} - t_{c,i}^{\tau}) \tag{4}$$

$$A_{c,i} = \pi D \Delta l_i \tag{5}$$

where $D$ is the inner diameter of the copper pipe; $\rho_r$ is the density of the refrigerant; $h_{r\text{-}in}$ and $h_{r\text{-}out}$ are the inlet and outlet enthalpies of the refrigerant; $\tau$ is the time; $G_r$ is the mass flow rate of the refrigerant; $\alpha_r$ is the convective heat transfer coefficient of the refrigerant; $A_c$ is the inner surface area of the copper pipe; $t_r$ is the temperature of the refrigerant; $t_c$ is the temperature of the copper pipe.

Journal Pre-proofs

As the refrigerant flows in copper pipes, the state of the refrigerant will change and the corresponding convective heat transfer coefficient will change as well. When the refrigerant is in single-phase region, its convective heat transfer coefficient can be defined as [26]:

$$\alpha_{\mathrm{r},i} = Nu_{\mathrm{r},i}\frac{\lambda_{\mathrm{r},i}}{D} \tag{6}$$

$$Nu_{\mathrm{r},i}=0.023Re_{\mathrm{r},i}^{0.8}Pr_{\mathrm{r},i}^{1/3} \tag{7}$$

$$Re_{\mathrm{r},i} = \frac{\rho_{\mathrm{r},i}u_{\mathrm{r},i}D}{\mu_{\mathrm{r},i}} \tag{8}$$

$$Pr_{\mathrm{r},i} = \frac{\mu_{\mathrm{r},i}c_{p\mathrm{r},i}}{\lambda_{\mathrm{r},i}} \tag{9}$$

where $Nu_{\mathrm{r}}$ is the Nusselt number of the refrigerant; $\lambda_{\mathrm{r}}$ is the thermal conductivity of the refrigerant; $Re_{\mathrm{r}}$ and $Pr_{\mathrm{r}}$ are the Reynolds number and the Prandtl number of the refrigerant; $u_{\mathrm{r}}$ and $\mu_{\mathrm{r}}$ are the flow velocity and dynamic viscosity of the refrigerant; $c_{p\mathrm{r}}$ is the specific heat of the refrigerant.

When the refrigerant is in two-phase region, its temperature is regarded as condensing temperature. The convective heat transfer coefficient of the refrigerant is determined as [27]:

$$\alpha_{\mathrm{r},i} = \psi_{\mathrm{r},i}\cdot\alpha_{\text{r-cond},i} \tag{10}$$

$$\alpha_{\text{r-cond},i}=\alpha_{\mathrm{rl},i}(1-x_i)^{0.8} \tag{11}$$

$$\alpha_{\mathrm{rl},i}=0.023Re_{\mathrm{rl},i}^{0.8}Pr_{\mathrm{rl},i}^{1/3}\frac{\lambda_{\mathrm{rl},i}}{D} \tag{12}$$

$$Re_{\mathrm{rl},i} = \frac{\rho_{\mathrm{rl},i}u_{\mathrm{rl},i}D}{\mu_{\mathrm{rl},i}} \tag{13}$$

$$Pr_{\mathrm{rl},i} = \frac{\mu_{\mathrm{rl},i}c_{p\mathrm{rl},i}}{\lambda_{\mathrm{rl},i}} \tag{14}$$

Journal Pre-proofs

where $\alpha_{\text{r-cond}}$ is the condensation heat transfer coefficient of the refrigerant; $\alpha_{\text{rl}}$ is the convection heat transfer coefficient of the refrigerant in liquid phase; $x$ is the vapor quality of the refrigerant; $Re_{\text{rl}}$ and $Pr_{\text{rl}}$ are the Reynolds number and Prandtl number of the refrigerant in liquid phase; $\lambda_{\text{rl}}$ is the thermal conductivity of the refrigerant in liquid phase; $\rho_{\text{rl}}$ is the density of the refrigerant in liquid phase; $u_{\text{rl}}$ and $\mu_{\text{rl}}$ are the flow velocity and dynamic viscosity of the refrigerant in liquid phase; $c_{p\text{rl}}$ is the specific heat of the refrigerant in liquid phase; $\psi_{\text{r}}$ is the flow coefficient of the refrigerant, which is proposed by Shah [28], and the expression is written as:

$$\psi_{\text{r},i}=1+\frac{3.8}{C_{\text{r},i}^{0.95}} \tag{15}$$

$$C_{\text{r},i}=(\frac{1}{x_i}-1)^{0.8}\Delta p_{\text{r},i}^{0.4} \tag{16}$$

$$\Delta p_{\text{r},i}=\frac{p_{\text{r},i}}{p_{\text{cr},i}} \tag{17}$$

where $C_{\text{r}}$ is correlation coefficient of the refrigerant; $\Delta p_{\text{r}}$ is the pressure drop of the refrigerant; $p_{\text{r}}$ is the pressure of the refrigerant; $p_{\text{rc}}$ is the critical pressure of the refrigerant.

2.2.2 Heat transfer of the copper pipe, aluminum foil and CPCM module package shell

Since the copper pipe, aluminum foil and CPCM module package shell are metal materials and the thicknesses of them are petty, the above sections are considered as a whole control volume. The heat of this control volume is composed of the heat change in the control volume $Q_{\text{mc}}$, convective heat transfer between this control volume and refrigerant $Q_{\text{r-c}}$, heat conduction between this control volume and CPCM module $Q_{\text{m-CPCM}}$ and heat conduction between this control volume and composite floor $Q_{\text{m-f}}$, which

Journal Pre-proofs

can be defined as:

$$Q_{\mathrm{mc}} = Q_{\mathrm{r\text{-}c}} - Q_{\mathrm{m\text{-}CPCM}} - Q_{\mathrm{m\text{-}f}} \tag{18}$$

$$Q_{\mathrm{mc}} = \frac{\left[c_{pc,i}\rho_{\mathrm{c},i}A_{\mathrm{c},i} + c_{p\mathrm{al\text{-}s},i}\rho_{\mathrm{al\text{-}s},i}(A_{\mathrm{al},i} + A_{\mathrm{s},i})\right]\Delta l_i(t_{\mathrm{c},i}^{\tau} - t_{\mathrm{c},i}^{\tau-\Delta\tau})}{\Delta\tau} \tag{19}$$

$$A_{\mathrm{c},i} = \pi(\frac{D_{\mathrm{w}}}{2})^2 - \pi(\frac{D}{2})^2 \tag{20}$$

$$A_{\mathrm{al},i} = \pi(\frac{D_{\mathrm{w}} + \delta_{\mathrm{al}}}{2})^2 - \pi(\frac{D_{\mathrm{w}}}{2})^2 \tag{21}$$

$$A_{\mathrm{s},i} = \pi(\frac{D_{\mathrm{w}} + \delta_{\mathrm{al}} + \delta_{\mathrm{s}}}{2})^2 - \pi(\frac{D_{\mathrm{w}} + \delta_{\mathrm{al}}}{2})^2 \tag{22}$$

where $c_{p\mathrm{c}}$ is the specific heat of the copper pipe; $\rho_{\mathrm{c}}$ is the density of the copper pipe; $c_{p\mathrm{al\text{-}s}}$ is the comprehensive specific heat of the aluminum foil and CPCM module package shell; $\rho_{\mathrm{al\text{-}s}}$ is the comprehensive density of the aluminum foil and CPCM module package shell; $A_{\mathrm{al}}$ is the annular cross-sectional area of the aluminum foil wrapped copper pipe; $A_{\mathrm{s}}$ is the annular cross-sectional area at the groove of the CPCM module package shell; $D_{\mathrm{w}}$ is the outer diameter of the copper pipe; $\delta_{\mathrm{al}}$ is the thickness of the aluminum foil; $\delta_{\mathrm{s}}$ is the thickness of the CPCM module package shell.

The $Q_{\mathrm{r\text{-}c}}$ is calculated by Eq. (4), and the $Q_{\mathrm{m\text{-}CPCM}}$ is made up of two components: heat conduction between CPCM module package shell without groove and CPCM module $Q'_{\mathrm{m\text{-}CPCM}}$, and heat conduction between the groove of the CPCM module package shell and CPCM module $Q''_{\mathrm{m\text{-}CPCM}}$, which can be formulated as [29]:

$$Q_{\mathrm{m\text{-}CPCM}} = Q'_{\mathrm{m\text{-}CPCM}} + Q''_{\mathrm{m\text{-}CPCM}} \tag{23}$$

$$Q'_{\mathrm{m\text{-}CPCM}} = 2\sqrt{\lambda_{\mathrm{s}}\lambda_{\mathrm{s\text{-}CPCM}}U_{\mathrm{sk}}A_{\mathrm{sk}}}\theta_{\mathrm{sk},i}th(m_{\mathrm{sk}}H_{\mathrm{sk}}) \tag{24}$$

$$U_{\mathrm{sk}} = 2\Delta l \tag{25}$$

$$A_{\mathrm{sk}} = \Delta l\delta_{\mathrm{sk}} \tag{26}$$

$$\theta_{\mathrm{sk},i} = t_{\mathrm{c},i} - t_{\mathrm{CPCM},i} \tag{27}$$

Journal Pre-proofs

$$m_{\mathrm{sk}}=\sqrt{\frac{2\lambda_{\mathrm{s\text{-}CPCM}}}{\lambda_{\mathrm{s}}\delta_{\mathrm{sk}}}} \tag{28}$$

$$H_{\mathrm{sk}}=l_{\mathrm{s}}+w_{\mathrm{s}}-\frac{1}{2}D_{\mathrm{w}}-\delta_{\mathrm{al}} \tag{29}$$

where $\lambda_{\mathrm{s}}$ is the thermal conductivity of the CPCM module package shell; $\lambda_{\mathrm{s\text{-}CPCM}}$ is the comprehensive thermal conductivity of the CPCM module package shell and CPCM module; $U_{\mathrm{sk}}$ and $A_{\mathrm{sk}}$ are the perimeter and cross-sectional area of the CPCM module package shell without groove; $\theta_{\mathrm{sk}}$ is the excess temperature between copper pipe and CPCM module; $H_{\mathrm{sk}}$ and $\delta_{\mathrm{sk}}$ are the height and thickness of the CPCM module package shell without groove; $t_{\mathrm{CPCM}}$ is the temperature of the CPCM module; $l_{\mathrm{s}}$ and $w_{\mathrm{s}}$ are the length and width of the CPCM module package shell. The $Q''_{\mathrm{m\text{-}CPCM}}$ is given as:

$$Q''_{\mathrm{m\text{-}CPCM}}=A_{\mathrm{s\text{-}CPCM}}\frac{t^{\tau}_{\mathrm{c},i}-t^{\tau}_{\mathrm{CPCM},i}}{\frac{\delta_{\mathrm{s}}}{2\lambda_{\mathrm{s}}}+\frac{\delta_{\mathrm{CPCM}}}{2\lambda_{\mathrm{CPCM}}}} \tag{30}$$

$$A_{\mathrm{s\text{-}CPCM}}=\pi(D_{\mathrm{w}}+2\delta_{\mathrm{al}}+2\delta_{\mathrm{s}})\Delta l \tag{31}$$

$$\delta_{\mathrm{CPCM}}=\frac{4l_{\mathrm{s}}w_{\mathrm{s}}}{2(l_{\mathrm{s}}+w_{\mathrm{s}})} \tag{32}$$

where $A_{\mathrm{s\text{-}CPCM}}$ is the contact area between the groove of the CPCM module package shell and CPCM module; $\delta_{\mathrm{CPCM}}$ is the thickness of the CPCM module; $\lambda_{\mathrm{CPCM}}$ is the thermal conductivity of the CPCM module.

The $Q_{\mathrm{m\text{-}f}}$ can be described as:

$$Q_{\mathrm{m\text{-}f}}=2\sqrt{\lambda_{\mathrm{al}}\lambda_{\mathrm{al\text{-}f}}U_{\mathrm{al}}A_{\mathrm{al}}}\theta_{\mathrm{al},i}th(m_{\mathrm{al}}H_{\mathrm{al}}) \tag{33}$$

$$U_{\mathrm{al}}=2\Delta l \tag{34}$$

$$A_{\mathrm{al}}=\Delta l\delta_{\mathrm{al}} \tag{35}$$

$$\theta_{\mathrm{al},i}=t_{\mathrm{c},i}-t_{\mathrm{f},i} \tag{36}$$

Journal Pre-proofs

$$m_{\mathrm{al}}=\sqrt{\frac{2\lambda_{\mathrm{al\text{-}f}}}{\lambda_{\mathrm{al}}\delta_{\mathrm{al}}}} \tag{37}$$

$$H_{\mathrm{al}}=\frac{1}{2}(l_{\mathrm{s}}-D_{\mathrm{w}}) \tag{38}$$

where $\lambda_{\mathrm{al}}$ is the thermal conductivity of the aluminum foil; $\lambda_{\mathrm{al\text{-}f}}$ is the comprehensive thermal conductivity of the aluminum foil and composite floor; $U_{\mathrm{al}}$ and $A_{\mathrm{al}}$ are the perimeter and cross-sectional area of the aluminum foil; $\theta_{\mathrm{al}}$ is the excess temperature between copper pipe and composite floor; $H_{\mathrm{al}}$ is the height of the aluminum foil; $t_{\mathrm{f}}$ is the temperature of the composite floor.

2.2.3 Heat transfer of the CPCM module

The heat of the CPCM module is comprised of the heat exchange in the control volume $Q_{\mathrm{CPCMc}}$, heat conduction between CPCM module and copper pipe, aluminum foil as well as CPCM module package shell $Q_{\mathrm{m\text{-}CPCM}}$ and heat storage capacity of the CPCM module $Q_{\mathrm{CPCMst}}$, and the expression is determined as:

$$Q_{\mathrm{CPCMc}}=Q_{\mathrm{m\text{-}CPCM}}-Q_{\mathrm{CPCMst}} \tag{39}$$

$$Q_{\mathrm{CPCMc}}=\frac{c_{p\mathrm{CPCM}}\rho_{\mathrm{CPCM}}\left[(l_{\mathrm{s}}-\delta_{\mathrm{s}})(w_{\mathrm{s}}-\delta_{\mathrm{s}})-\pi(\frac{D_{\mathrm{w}}}{2}+\delta_{\mathrm{al}}+\delta_{\mathrm{s}})^2\right]\Delta l(t^{\tau}_{\mathrm{CPCM},i}-t^{\tau-\Delta\tau}_{\mathrm{CPCM},i})}{\Delta\tau} \tag{40}$$

where $c_{p\mathrm{CPCM}}$ is the specific heat of the CPCM module; $\rho_{\mathrm{CPCM}}$ is the density of the CPCM module.

The $Q_{\mathrm{m\text{-}CPCM}}$ can be obtained by Eq. (23), and the $Q_{\mathrm{CPCMst}}$ is defined as:

$$Q_{\mathrm{CPCMst}}=m_{\mathrm{CPCM}}La_{\mathrm{CPCM}}\frac{(f^{\tau}_{\mathrm{CPCM},i}-f^{\tau-\Delta\tau}_{\mathrm{CPCM},i})}{\Delta\tau} \tag{41}$$

$$f_{\mathrm{CPCM}}=\frac{t_{\mathrm{CPCMme}}-t^{\tau}_{\mathrm{CPCM},i}}{t_{\mathrm{CPCMme}}-t_{\mathrm{CPCMso}}} \tag{42}$$

Journal Pre-proofs

where $m_{\mathrm{CPCM}}$ is the weight of the CPCM module; $La_{\mathrm{CPCM}}$ is the latent heating capacity of the CPCM module; $t_{\mathrm{CPCMme}}$ is the initial melting temperature of the CPCM module; $t_{\mathrm{CPCMso}}$ is the initial solidification temperature of the CPCM module; $f_{\mathrm{CPCM}}$ is the solid fraction of the CPCM module, $f_{\mathrm{CPCM}} = 0$ represents the phase change material in liquid phase, $f_{\mathrm{CPCM}} = 1$ represents the phase change material in solid phase, and $0 < f_{\mathrm{CPCM}} < 1$ represents the phase change material in solid-liquid two-phase. During the solidification process, the $f_{\mathrm{CPCM}}$ ascends with the increase of time. During the melting process, the change of the $f_{\mathrm{CPCM}}$ is opposite.

2.2.4 Heat transfer of the composite floor

The heat of the composite floor including the heat change in the control volume $Q_{\mathrm{fc}}$, heat transfer between composite floor and copper pipe, aluminum foil as well as CPCM module package shell $Q_{\mathrm{m\text{-}f}}$ and heat transfer between composite floor and indoor environment $Q_{\mathrm{f\text{-}n}}$, which is determined as:

$$Q_{\mathrm{fc}} = Q_{\mathrm{m\text{-}f}} - Q_{\mathrm{f\text{-}n}} \tag{43}$$

$$Q_{\mathrm{fc}} = \frac{c_{p\mathrm{f}} \rho_{\mathrm{f}} \delta_{\mathrm{f}} \Delta l (t_{\mathrm{f},i}^{\tau} - t_{\mathrm{f},i}^{\tau-\Delta\tau})}{\Delta\tau} \tag{44}$$

where $c_{p\mathrm{f}}$ is the specific heat of the composite floor; $\rho_{\mathrm{f}}$ is the density of the composite floor; $\delta_{\mathrm{f}}$ is the thickness of the composite floor.

The formula of the $Q_{\mathrm{m\text{-}f}}$ is the same as Eq. (33), and the $Q_{\mathrm{f\text{-}n}}$ consists of the convective heat transfer between composite floor and indoor environment $Q_{\mathrm{f\text{-}n,conv}}$ and radiant heat transfer between composite floor and indoor environment $Q_{\mathrm{f\text{-}n,rad}}$, which can be given as [30]:

Journal Pre-proofs

$$Q_{\text{f-n}} = Q_{\text{f-n,conv}} + Q_{\text{f-n,rad}} \tag{45}$$

$$Q_{\text{f-n,conv}} = \alpha_{\text{f-n,conv}} A_{\text{f},i} (t^{\tau}_{\text{f},i} - t_{\text{n}}) \tag{46}$$

$$\alpha_{\text{f-n,conv}} = Nu_{\text{n}} \frac{\lambda_{\text{n}}}{Z_{\text{f}}} \tag{47}$$

$$Nu_{\text{n}} = 0.15 Ra_{\text{n}}^{1/3} \tag{48}$$

$$Ra_{\text{n}} = Gr_{\text{n}} \cdot \text{Pr}_{\text{n}} \tag{49}$$

$$Gr_{\text{n}} = \frac{g \beta_{\text{n}} (t_{\text{f},i} - t_{\text{n}}) Z_{\text{f}}^3}{\nu_{\text{n}}^2} \tag{50}$$

$$\beta_{\text{n}} = \frac{1}{(t_{\text{f}} + t_{\text{n}})/2 + 273.15} \tag{51}$$

$$Pr_{\text{n}} = \frac{\nu_{\text{n}}}{a_{\text{n}}} \tag{52}$$

where $\alpha_{\text{f-n,conv}}$ is the convective heat transfer coefficient between composite floor and indoor environment; $A_{\text{f}}$ is the surface area of the composite floor; $t_{\text{n}}$ is the indoor air temperature; $Nu_{\text{n}}$ and $Ra_{\text{n}}$ are the Nusselt number and Rayleigh number of the indoor air; $Gr_{\text{n}}$ and $Pr_{\text{n}}$ are the Grashov number and Prandtl number of the indoor air; $\lambda_{\text{n}}$ is the thermal conductivity of the indoor air; $Z_{\text{f}}$ is the characteristic length, which is equal to the average value of the length and width of the composite floor; $\beta_{\text{n}}$ is the volume expansion coefficient of the indoor air; $\nu_{\text{n}}$ is the kinematic viscosity of the indoor air; $a_{\text{n}}$ is the thermal diffusivity of the indoor air.

The $Q_{\text{f-n,rad}}$ can be evaluated by:

$$Q_{\text{f-n,rad}} = \alpha_{\text{f-n,rad}} A_{\text{f},i} (t^{\tau}_{\text{f},i} - t_{\text{nh}}) \tag{53}$$

$$\alpha_{\text{f-n,rad}} = \varepsilon_{\text{f}} \sigma \left[ (t^{\tau}_{\text{f},i} + 273.15)^2 + (t_{\text{nh}} + 273.15)^2 \right] \left[ (t^{\tau}_{\text{f},i} + 273.15) + (t_{\text{nh}} + 273.15) \right] \tag{54}$$

Journal Pre-proofs

$$t_{\mathrm{nh}}=\frac{\sum_{j=1}^{5}A_{\mathrm{nh},j}t_{\mathrm{nh},j}}{\sum_{j=1}^{5}A_{\mathrm{nh},j}} \tag{55}$$

where $\alpha_{\mathrm{f\text{-}n,rad}}$ is the radiant heat transfer coefficient between composite floor and indoor building envelope; $t_{\mathrm{nh}}$ is the non-heating surface temperature of the test room; $\varepsilon_{\mathrm{f}}$ is the emissivity of the composite floor; $\sigma$ is the Stefan-Boltzmann constant, $5.67\lozenge10^{-8}$ W· m$^{-2}$· K$^{-4}$; $A_{\mathrm{nh}}$ is the non-heating surface area of the test room.

*2.3 Solution procedure*

The solution procedure of the numerical model of the RFHC is depicted in Fig. 3. The calculation steps are as follow: (a) input geometrical and physical parameters of the RFHC, indoor air temperature, refrigerant inlet temperature, refrigerant mass flow rate and time step; (b) assume the initial value of the refrigerant temperature $t'_{\mathrm{r},i}$; (c) calculate the convective and radiant heat transfer coefficients, and produce the coefficient matrix $\boldsymbol{B}$ and constant vector $\boldsymbol{b}$, and then calculate the refrigerant temperature $t_{\mathrm{r},i}$, the comprehensive temperature of the copper pipe, aluminum foil and CPCM module package shell $t_{\mathrm{m},i}$, CPCM module temperature $t_{\mathrm{CPCM},i}$ and composite floor temperature $t_{\mathrm{f},i}$; (d) if the difference between calculated refrigerant temperature and assumed value is less than 0.01 $^{\mathrm{o}}$C, the iteration will be suspended. Otherwise, re-assume the $t'_{\mathrm{r},i}$ and recalculate until the convergence condition is met. During the iterative process, when the $t_{\mathrm{r},i} > t_{\mathrm{r,sat}}$ or $t_{\mathrm{r},i} < t_{\mathrm{r,sat}}$, the refrigerant is in single-phase region. When the $t_{\mathrm{r},i} = t_{\mathrm{r,sat}}$, the refrigerant enters the two-phase region.

Journal Pre-proofs

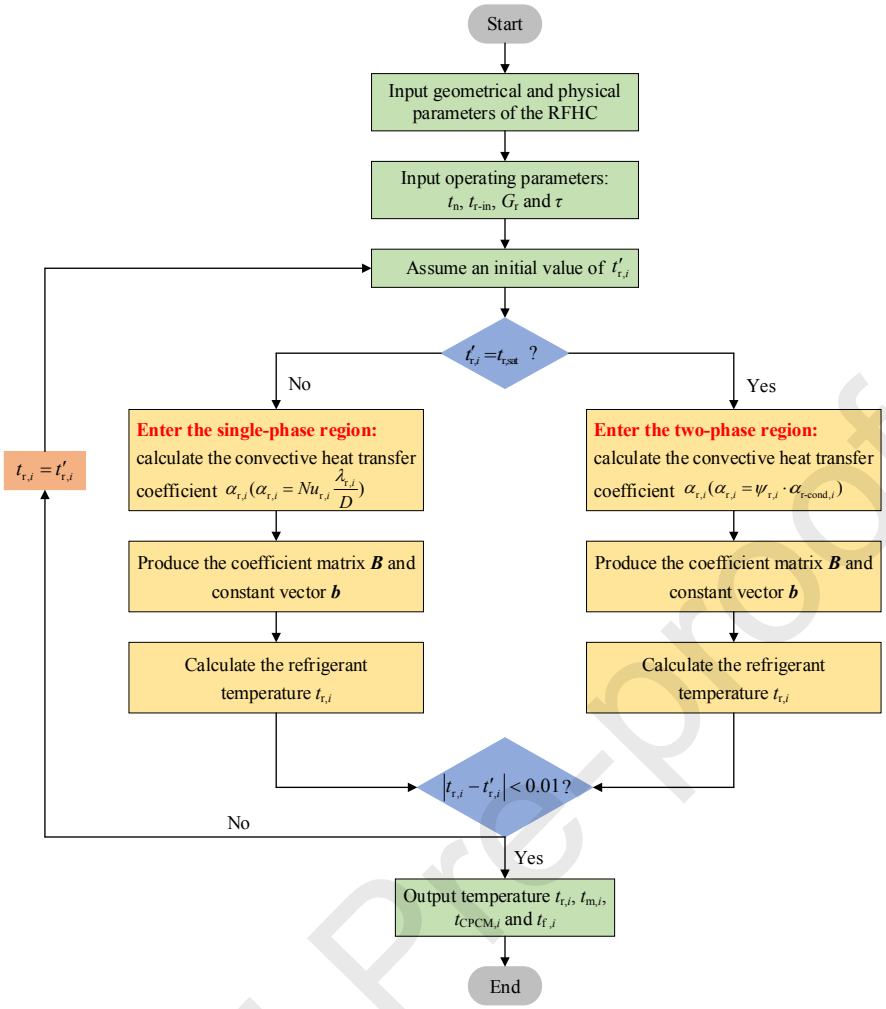


Fig. 3. The solution procedure of the numerical model of the RFHC.

## 3. Experimental test

### *3.1 The experimental system*

The experiment of the RFHC system is conducted in a laboratory, including indoor-environmental chamber and outdoor-environmental chamber, as shown in Fig. 4. The climate chamber of constant temperature-humidity is used to simulate indoor environment, which depends on the top orifice for air supply. The outdoor-environmental chamber is built of polyurethane insulation board, and the air cooler and humidifier are installed to maintain its thermal environment. To avoid forced

Journal Pre-proofs

convection, a test room with metal shell is constructed in the indoor-environmental chamber. The RFHC system consists of a compressor, a four-way valve, a gas-liquid separator, the RFHC (condenser), a throttling valve, an evaporator and connecting tubes. During the test, the refrigerant is compressed by the compressor and then condensed by the RFHC, then passed through the throttling valve and sent to the evaporator. At last, the refrigerant flows back to the compressor for a new cycle. In the RFHC system, the composite floor surface temperature depends on the condensing temperature, and the condensing temperature is determined by compressor frequency, opening of expansion valve and fan setting value. The above parameters are regulated by PID controller. The indoor air temperature, composite floor surface temperature, interior wall surface temperature, outdoor ambient temperature are measured by copper-constantan thermocouples. The indoor and outdoor relative humidity are measured by humidity sensors. The suction and discharge temperatures of the compressor, and the pressures and temperatures of the RFHC and evaporator are monitored by the control panel. The power consumption of this system is recorded by a watt-hour meter. The measuring instruments and accuracies are list in Table 1.

Table. 1 Specifications of measuring instruments.

| Measured parameters | Instruments | Type | Full scales | Accuracies |
|---|---|---|---|---|
| temperature | copper-constantan thermocouple | PT 100 | -50 – 150 $^{o}$C | ± 0.5 $^{o}$C |
| relative humidity | humidity sensor | Testo 175 H1 | 0 – 100% RH | ± 2% RH |
| pressure | pressure transmitter | MIK-P300 | -0.1 – 1.8 MPa | 9.5 kPa |
| mass flow rate | Coriolis mass flowmeter | KLB-CF1-DN6 | 0 – 700 kg· $h^{-1}$ | ± 0. 2 kg· $h^{-1}$ |
| electric power | power meter | - | 0. 1 – 999 kW | ± 0.01 kW |

Journal Pre-proofs

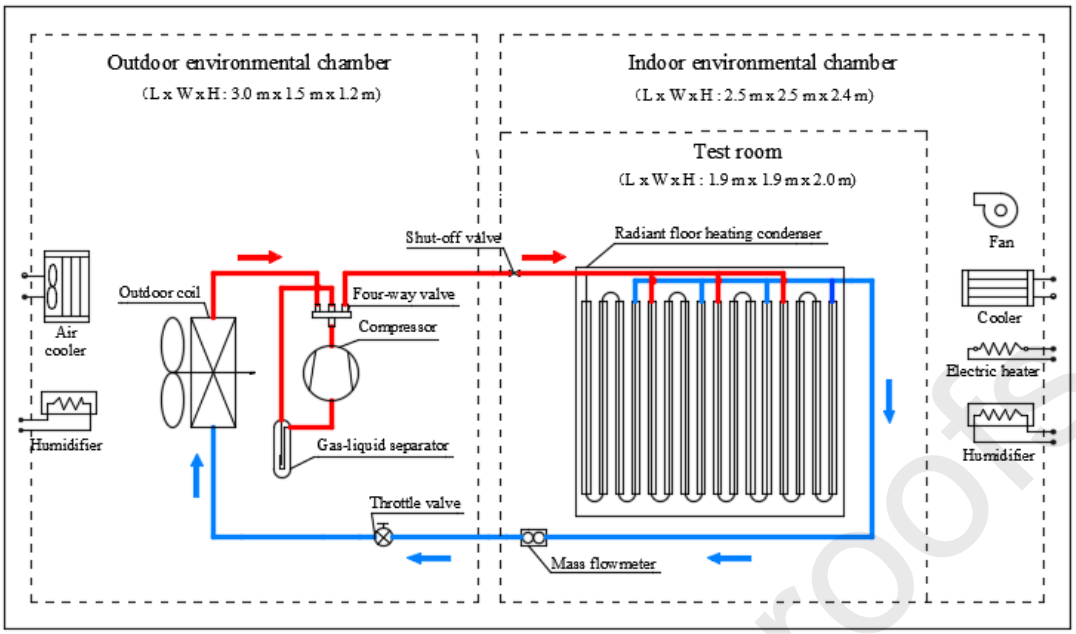


Fig. 4. The experimental system of the RFHC.

The layout of measuring points in the test room is shown in Fig. 5. Four measuring points are set up at the central axis to monitor the indoor air temperature, which are located at the height of 0.1 m, 0.75 m, 1.5 m and 1.9 m. The measured temperature of 0.75 m is considered as reference point temperature. Five measuring points are arranged at roof and four walls to reflect its thermal environment. Ten measuring points are uniformly distributed on the composite floor and their arithmetic mean value is regarded as mean temperature of composite floor surface. In order to avoid the thermal radiation, the protection treatment is carried out for measuring points.

Fig. 5. The layout of measuring points in the test room.

Journal Pre-proofs

*3.2 System performance analysis*

Taking the condensing temperature of 38.0 °C as an example, the changes of the condensing pressure and temperature, evaporating pressure and temperature, and compressor discharge temperature are illustrated in Fig. 6. Under the outdoor air temperature of 4.1 °C ~ 6.3 °C, the operating parameters vary acutely about 30 minutes then tend to be steady. The condensing pressure and temperature increase intensely and then decline, and finally stabilize at $22.0\times10^5$ Pa and 38.0 °C. Correspondingly, the compressor discharge temperature rises rapidly to 65.0 °C and then drops, and finally maintains at 43.0 °C. While the evaporating pressure and temperature show the opposite tends, which decline sharply first and then increase, and finally remain at $8.2\times10^5$ Pa and 5.0 °C. The variation trends of the inlet and outlet temperatures of the RFHC, composite floor surface temperature and indoor air temperature are described in Fig. 7. Both the inlet and outlet temperatures of the RFHC ascend obviously, and then stabilize at 38.4 °C and 35.1 °C. When the RFHC system operates for 16 minutes, the composite floor surface temperature grows up to 24.0 °C and maintains at 24.6 °C eventually. It is attributed that the copper pipes are in contact with the composite floor directly and has minor contact thermal resistance. Besides, the indoor air temperature increases slowly and finally remains at 18.0 °C. According to standard [31], the indoor air temperature is recommended to attain 18.0 °C in winter, which can be concluded that the RFHC system is able to meet the requirement.

Journal Pre-proofs

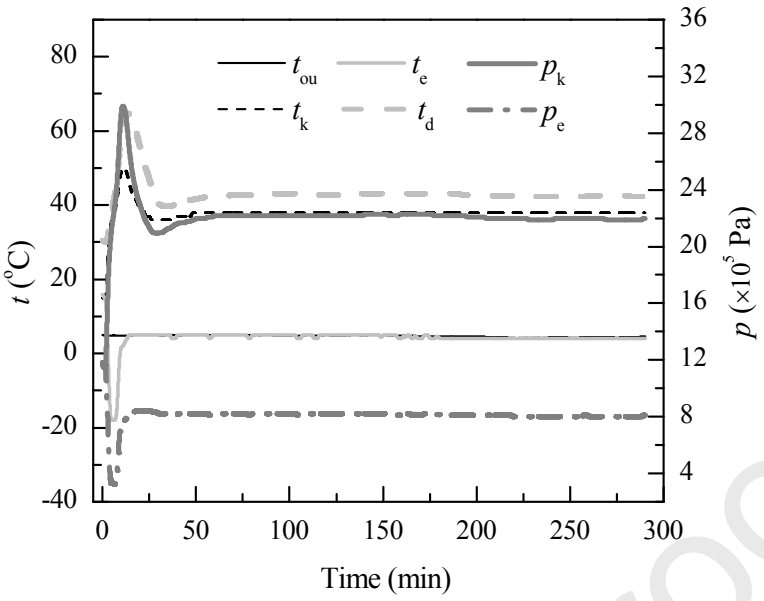


Fig. 6. The variations of operating parameters of the RFHC system.

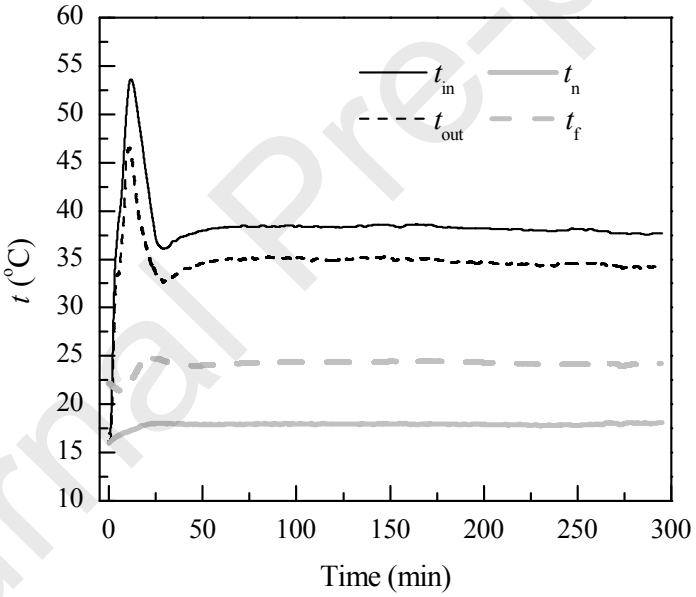


Fig. 7. The variations of different temperatures in operation.

The variation trends of composite floor surface temperatures, indoor air temperatures and heating capacities of the RFHC system with and without CPCM modules under defrosting condition are investigated. As shown in Fig. 8, all temperatures and heating capacities remain stable in the initial period. After defrosting

Journal Pre-proofs

for 6 minutes, the composite floor surface temperature with CPCM module decreases, which is 3 minutes later than that without CPCM module. When the systems defrosting are finished, the composite floor surface temperatures with and without CPCM module decline to 25.9 $^{o}$C and 24.2 $^{o}$C, and then their system enters the reheating stage separately. Meanwhile, the change trends of indoor air temperatures with and without CPCM module are similar to that of composite floor surface temperatures, while they need longer response time. During the whole defrosting process, the composite floor surface temperature and indoor air temperature with CPCM module are higher than that without CPCM module. It can be ascribed that the CPCM module releases a large amount of latent heat to provide heat for composite floor and indoor environment simultaneously.

In addition, both the heating capacities of the RFHC system with and without CPCM modules are declined in defrosting, and the descent rate of the system without CPCM module is higher than that of the system with CPCM module. When the systems defrosting are completed, the heating capacities with and without CPCM module are reduced to 233.3 W and 195.7 W. In the whole defrosting stage, the heating capacity of the RFHC system with CPCM module is larger than that of the system without CPCM module, with the average growth rate is 7.2%. This is due to the higher temperature of the composite floor surface with CPCM module. It can be concluded that the RFHC system with CPCM module has larger heating capacity and can reduce indoor air temperature fluctuation during defrosting.

Journal Pre-proofs

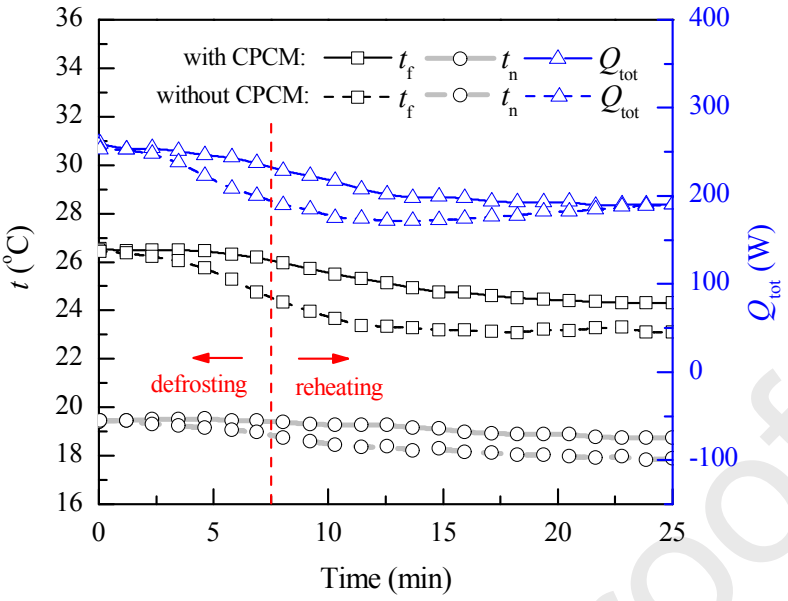


Fig. 8. The variations of different parameters of the RFHC system with and without CPCM modules.

*3.3 Comparison of COP*

When the indoor air temperature keeps at 18.0 °C and the outdoor air temperature remains at 7.0 °C, the COPs of the RFHC system and aluminium refrigerant-heated radiator (RHR) system are compared. As shown in Fig. 9, with the condensing temperature rises from 36.0 °C to 44.0 °C, the COP of this system deceases from 4.5 to 3.6 due to the increment of the power consumption. Compared with the aluminium RHR system, the COP of this system is within the range of 4.4 ~ 3.4 under the same operating conditions [32], which indicates that the RFHC system has more advantages in energy efficiency. The same conclusion is supported for the steel RHR system when the indoor air temperature keeps at 18.0 °C and the outdoor air temperature remains at 5.0 °C as well [33]. Both of the aluminium RHR system and steel RHR system adopt R410a refrigerant as circulating medium. It can be denoted that the RFHC system is conductive to improve the energy utilization.

Journal Pre-proofs

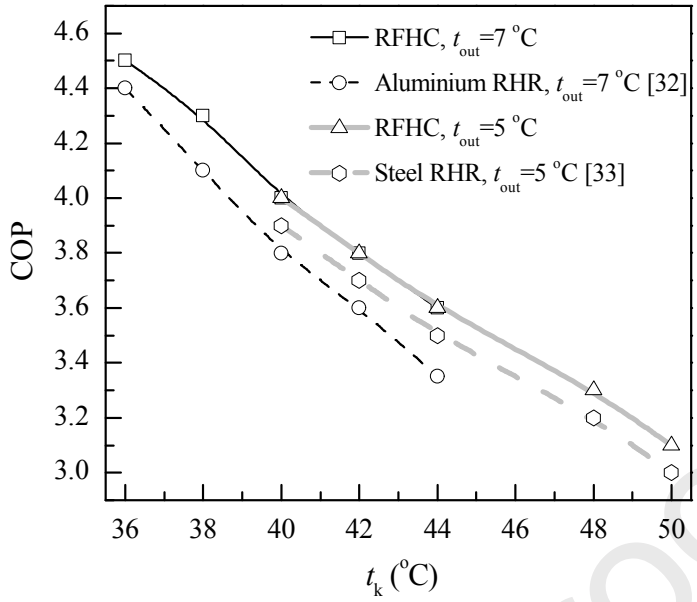


Fig. 9. The COPs of various ASHP systems under different condensing temperatures.

*3.4 Model validation*

The geometrical dimensions of the RFHC are depicted in Table 2. To determine the appropriate length of the control volume, it is necessary to verify the grid independence. When the indoor air temperature of 21.1 °C and the length of copper pipe of 12.0 m, the variation trend of heat flux with the number of grid is shown in Fig. 10. It is noted that if the number of grid is greater than 1500, the difference of calculated results is quite petty. Therefore, the number of grid with 2000 is selected for simulation of the RFHC system. The simulated results and experimental data of the composite floor surface temperature and heating capacity of this system are compared in Fig. 11. It can be found that the simulated results are in accordance with the measured data. The mean deviations of the composite floor surface temperature and heating capacity are 1.7% and 2.6%, and the maximum deviations of them are 2.5% and 6.5% due to the simplification of the numerical model and errors of the measuring instruments. It is indicated that the established numerical model is able to accurately predict the heat

Journal Pre-proofs

transfer performance of the RFHC system.

Table 2. The geometrical dimensions of the RFHC.

| Parameters | Dimensions (mm) | Parameters | Dimensions (mm) |
|---|---|---|---|
| $\delta_c$ | 0.5 | $D_w$ | 6.35 |
| $\delta_{al}$ | 0.2 | $Sp_c$ | 200.0 |
| $\delta_f$ | 8.0 | $l_c$ | $2.4\times10^4$ |

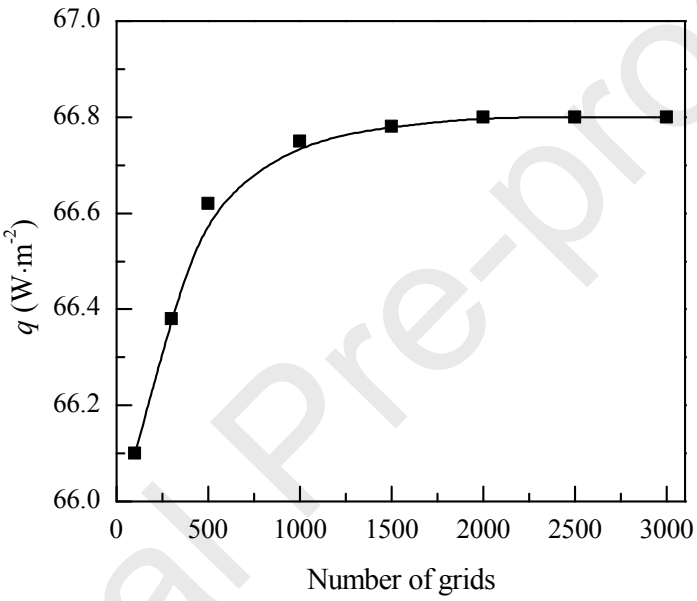


Fig. 10. Grid independence test.

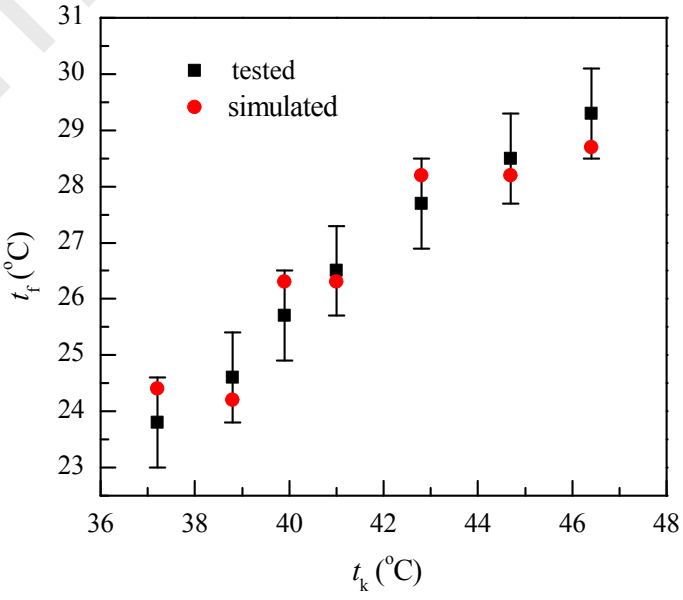


(a)

Journal Pre-proofs

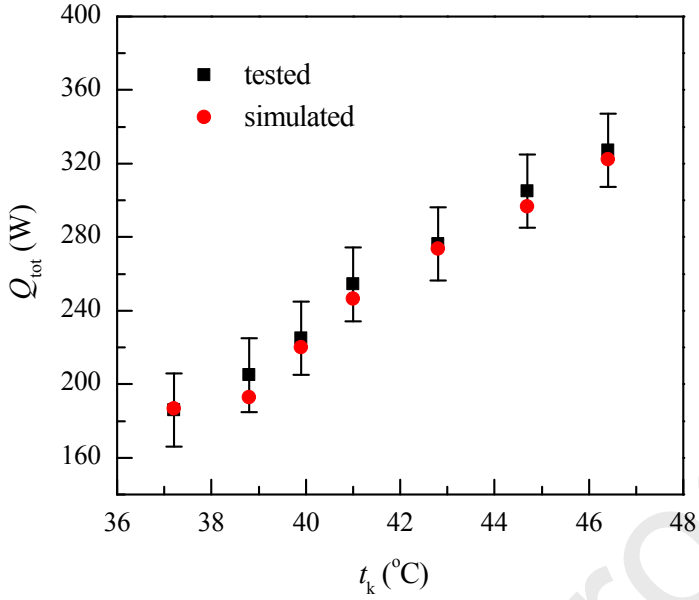


(b)

Fig. 11. Comparisons of the simulated results and experimental data of the RFHC system.

(a) composite floor surface temperature (b) heating capacity

## 4. Results and discussion

### *4.1 Effects of the operating parameters on heat transfer performance*

The copper pipes of the RFHC are divided into two parallel paths, and one branch is taken as an example for simulation. Under the condition of the indoor air temperature of test room with 18.0 °C, the copper pipe spacing with 0.25 m and the length of copper pipe with 12.0 m, the effects of the condensing temperature and refrigerant mass flow rate on the heat transfer performance of the RFHC system are investigated.

#### 4.1.1 Condensing temperature

When the refrigerant mass flow rate remains 4.0 kg· $h^{-1}$, the effect of the condensing temperature on the vapor quality of refrigerant at the outlet of the RFHC is

Journal Pre-proofs

examined. As shown in Fig. 12, if the condensing temperature is regulated at 38.0 °C, the vapor quality of refrigerant at the outlet of the RFHC is equal to 0, which illustrates that the refrigerant in copper pipes has entirely changed to liquid phase. When the condensing temperature is higher than 38.0 °C, the length of sub-cooled section of the refrigerant extends gradually, leading to the diminution of the refrigerant temperature.

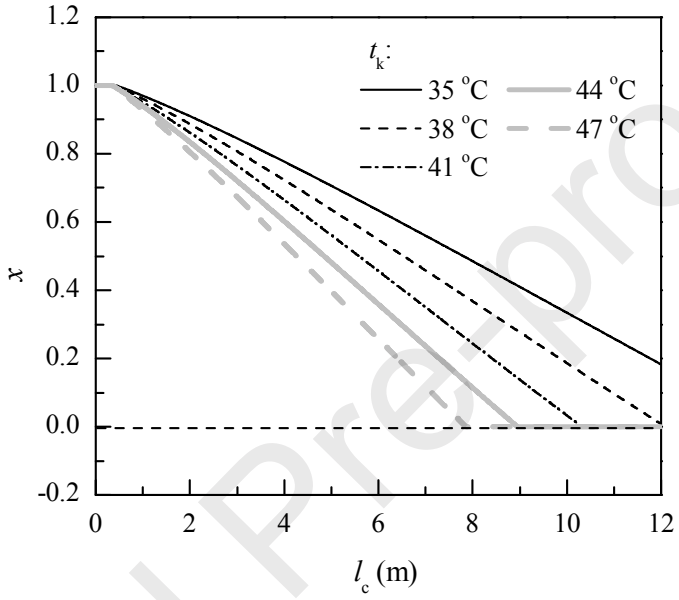


Fig. 12. The effect of condensing temperature on the vapor quality of refrigerant at the outlet.

Fig. 13 describes the variation trends of the composite floor surface temperature, heat flux and heating capacity of the RFHC system with the condensing temperature. As the condensing temperature increases from 35.0 °C to 47.0 °C, the composite floor surface temperature climbs from 23.3 °C to 25.5 °C due to the increment of the copper pipe temperature and aluminum foil temperature. Besides, the heating capacity ascends from 143.1 W to 204.4 W because the temperature difference between composite floor surface and indoor air goes up, and then the radiation and natural convection heating capacities enhance. The heat flux increases since the heat exchange area of the RFHC remains unchanged. However, the increment of the heating capacity declines

Journal Pre-proofs

continuously with the increase of the condensing temperature. When the condensing temperature varies from 44.0 °C to 47.0 °C, the heating capacity is only improved by 2.4%. In addition, the higher condensing temperature leads to higher energy consumption of the RFHC system. Thus, in the premise of providing sufficient heating capacity, the condensing temperature below 44.0 °C is a good choice for this system.

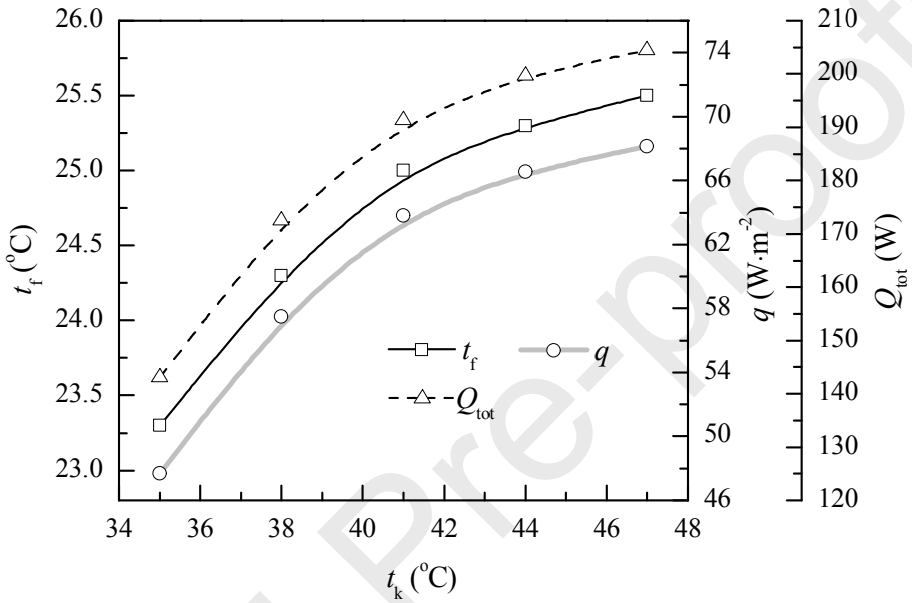


Fig. 13. The effect of the condensing temperature on heat transfer performance.

4.1.2 Refrigerant mass flow rate

When the condensing temperature maintains at 38.0 °C, the effect of the refrigerant mass flow rate on the vapor quality of refrigerant at the outlet of the RFHC is depicted in Fig. 14. As the refrigerant mass flow rate varies from 2.5 kg· h$^{-1}$ to 4.0 kg· h$^{-1}$, the vapor quality of refrigerant at the outlet of the RFHC is equal to 0. Correspondingly, the value is larger than 0 if the refrigerant mass flow rate exceeds 4.0 kg· h$^{-1}$, which illustrates that the refrigerant in copper pipes cannot be completely condensed. Besides, with the increase of the refrigerant mass flow rate, the length of sub-cooled section of

Journal Pre-proofs

the refrigerant shortens, and then the refrigerant temperature grows up.

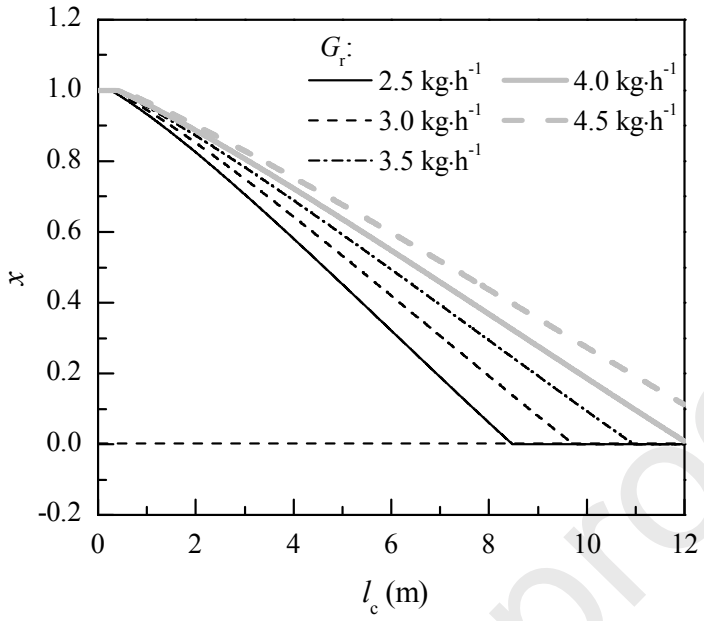


Fig. 14. The effect of the refrigerant mass flow rate on the vapor quality of refrigerant at the outlet.

With regard to Fig. 15, the changes of the composite floor surface temperature, heat flux and heating capacity of the RFHC system with the refrigerant mass flow rate are presented. The composite floor surface temperature ascends with the rise of the refrigerant mass flow rate owing to the elevation of the refrigerant temperature and aluminum foil temperature. The heating capacity improves from 121.2 W to 177.1 W, which is attributed that the refrigerant flow velocity accelerates, and the convective heat transfer coefficient between refrigerant and copper pipes ascends. Meanwhile, the heat flux raises because the heat exchange area of the RFHC is fixed. It is found that the heating capacity is barely improved by 2.7% when the refrigerant mass flow rate is within the range of 4.0 kg· h$^{-1}$ ~ 4.5 kg· h$^{-1}$. Therefore, it is suggested that the refrigerant mass flow rate of this system is less than 4.0 kg· h$^{-1}$ in operation.

Journal Pre-proofs

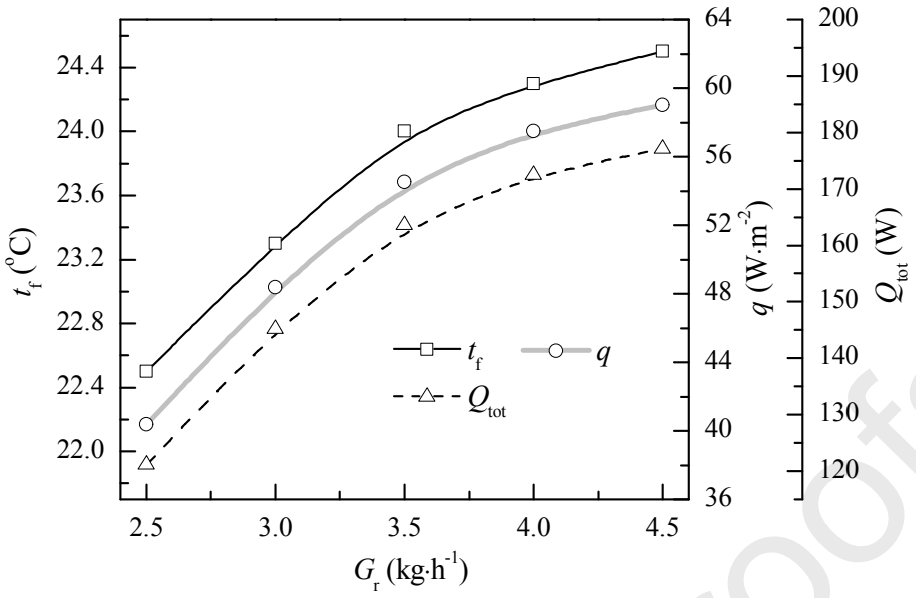


Fig. 15. The effect of the refrigerant mass flow rate on heat transfer performance.

*4.2 Effects of the structural parameters on heat transfer performance*

In the premise of the indoor air temperature with 18.0 °C, the condensing temperature with 38.0 °C and the refrigerant mass flow rate with 3.8 kg· h$^{-1}$, the effects of the copper pipe spacing and the length of copper pipe on the heat transfer performance of the RFHC system are studied.

4.2.1 Copper pipe spacing

When the length of copper pipe remains unchanged, the copper pipe spacing is a crucial factor affecting the heat transfer performance of the RFHC system. Fig. 16 depicts the change of the vapor quality of refrigerant at the outlet of the RFHC with the copper pipe spacing. As the copper pipe spacing rises from 0.1 m to 0.2 m, the vapor quality of refrigerant at the outlet of the RFHC is greater than 0, which indicates that the state of the refrigerant at the outlet of the RFHC is two-phase. If the copper pipe spacing is larger than 0.2 m, the state of the refrigerant at the outlet of the RFHC is

liquid phase and the vapor quality is equal to 0. It can be concluded that the copper pipe spacing exerts a significant role in the heat transfer performance of the RFHC system.

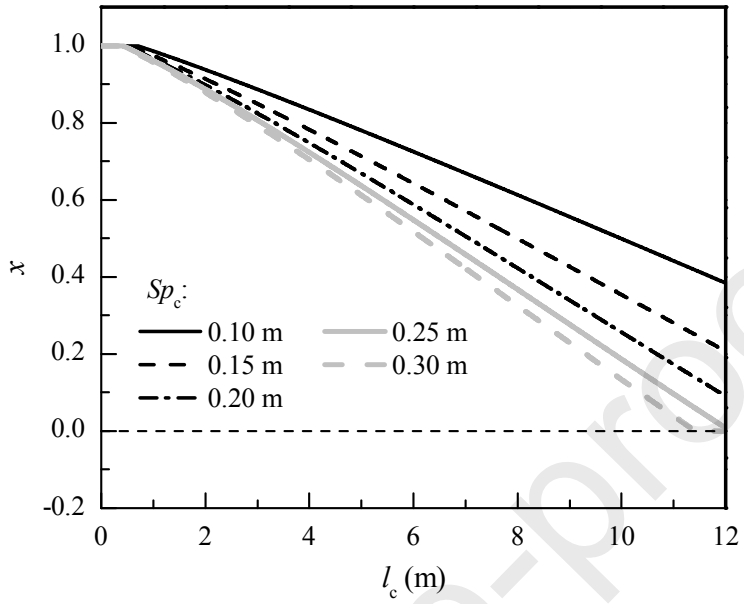


Fig. 16. The effect of the copper pipe spacing on the vapor quality of refrigerant at the outlet.

The effects of the copper pipe spacing on the composite floor surface temperature, heat flux and heating capacity of the RFHC system are described in Fig. 17. The composite floor surface temperature decreases since the length of sub-cooled section of the refrigerant goes up, resulting in the diminution of the refrigerant temperature. While the heating capacity grows up from 114.3 W to 178.9 W, which is attributed to the enhancement of the heat exchange area of the RFHC. When the copper pipe spacing varies from 0.1 m to 0.25 m, the heat flux is reduced by 39.6%, while the heating capacity is elevated by 50.9% since the heat exchange area of the RFHC is expanded twice. It can be denoted that the heat exchange area of the RFHC is a main contributor in heat transfer process. However, the increment of the heating capacity is merely increased by 3.7% if the copper pipe spacing is within the range of 0.25 m ~ 0.3 m. Therefore, the copper pipe spacing of the RFHC with 0.25 m is recommended.

Journal Pre-proofs

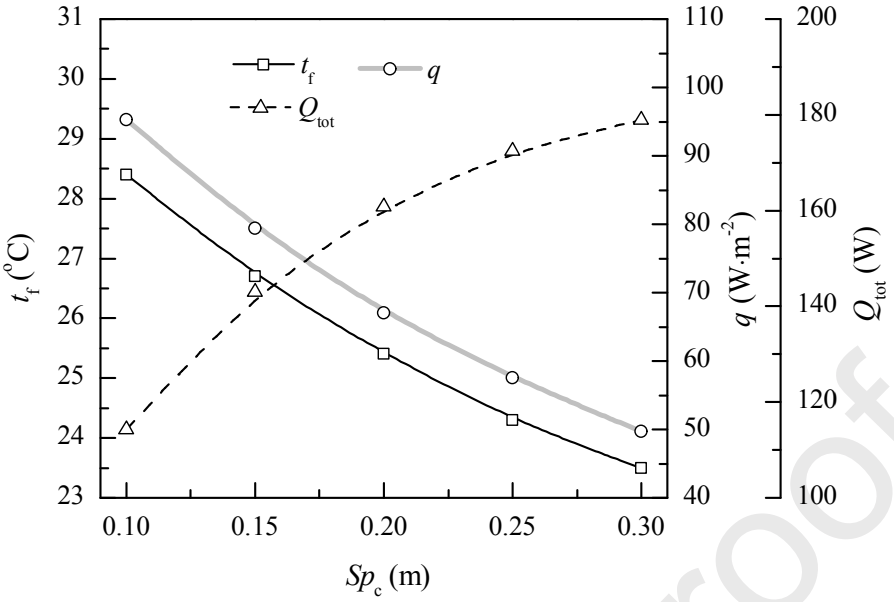


Fig. 17. The effect of the copper pipe spacing on heat transfer performance.

4.2.2 Length of copper pipe

To explore the effect of the length of copper pipe on the heat transfer performance of the RFHC system, the copper pipe spacing maintains at 0.25 m. The variation trend of the vapor quality of refrigerant at the outlet of the RFHC with the length of copper pipe is displayed in Fig. 18. The vapor quality of refrigerant at the outlet of the RFHC decreases rapidly and stabilizes at 0 with the rise of the length of copper pipe. When the length of copper pipe is larger than 12.0 m, the vapor quality of refrigerant at the outlet of the RFHC is equal to 0 and the state of the refrigerant at the outlet of the RFHC is liquid phase. Otherwise, the refrigerant in copper pipes cannot be thoroughly condensed and the state of the refrigerant at the outlet of the RFHC is two phase.

Journal Pre-proofs

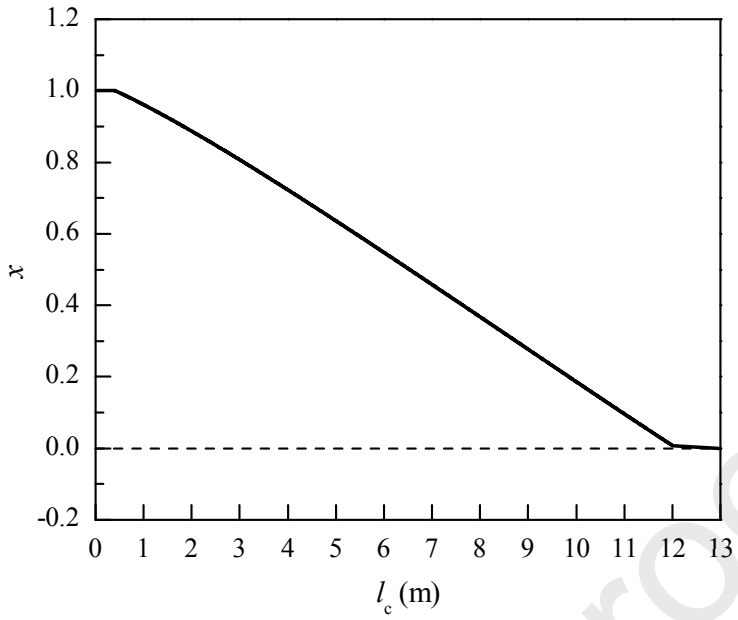


Fig. 18. The effect of the length of copper pipe on the vapor quality of refrigerant at the outlet.

Fig. 19 depicts the changes of the composite floor surface temperature, heat flux and heating capacity of the RFHC system with the increase of the length of copper pipe. The composite floor surface temperature remains constant then decreases, which is ascribed that when the length of copper pipe is larger than 12.0 m, the state of the refrigerant at the outlet of the RFHC is sub-cooled and the refrigerant temperature degrades gradually. The heating capacity improves obviously due to the enhancement of the heat exchange area of the RFHC. The heat flux varies slightly since the increment of the heating capacity with 43.8% is similar to that of the heat exchange area of the RFHC with 44.4%. However, as the length of copper pipe ascends from 12.0 m to 13.0 m, the growth rate of the heating capacity is merely 4.3%. Thus, in order to achieve the heat performance sufficiently, it is advisable to set the length of copper pipe of the RFHC with 12.0 m.

Based on the aforementioned analysis, it can be denoted that the condensing temperature with 38.0 $^{o}$C and the refrigerant mass flow rate with 3.8 kg· $h^{-1}$ of the RFHC

Journal Pre-proofs

system is the optimal operating condition. And the copper pipe spacing with 0.25 m and the length of copper pipe with 12.0 m of the RFHC is the optimal structural scheme.

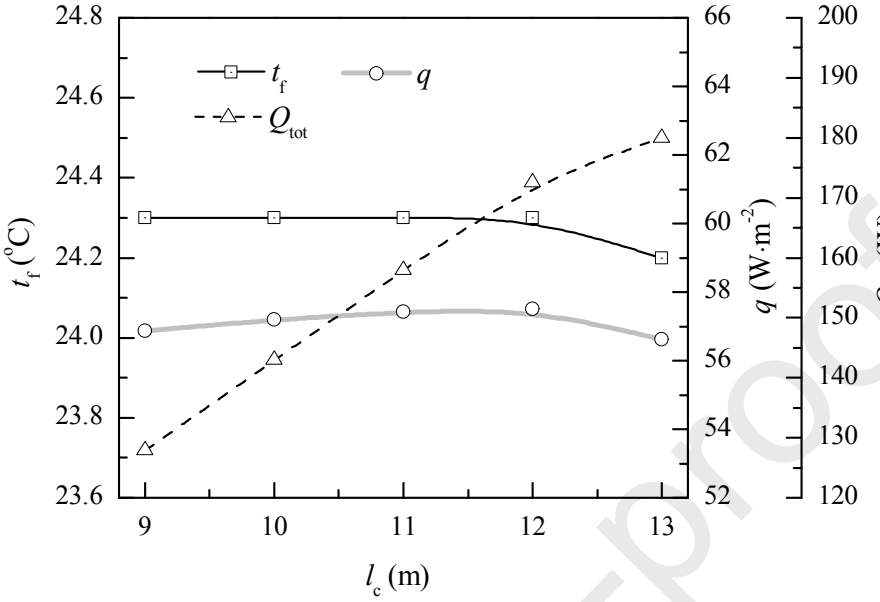


Fig. 19. The effect of the length of copper pipe on heat transfer performance.

## 5. Conclusion

To overcome the limitations of the existing ASHP systems, a novel heating system based on the RFHC with CPCM is proposed in this study. A numerical model of the RFHC is established and validated with the measured data. Based on the numerical model, the impacts of the operating and structural parameters on the heat transfer performance of the RFHC system are studied. The optimal operating condition and structural scheme are derived. The main conclusions are drawn as follows:

(1) When the RFHC system is used for space heating, the indoor air temperature is able to attain 18.0 °C, which illustrates that the proposed system is feasible and can undertake indoor heat load. Compared with the RFHC system without CPCM, the

proposed system is conductive to improve heating capacity and maintain the stability of indoor air temperature during defrosting.

(2) Under the same operating conditions, the COP of the RFHC system is higher than traditional ASHP systems, indicating that this system has a great potential in energy efficiency.

(3) The established numerical model of the RFHC is validated to be credible. The simulated composite floor temperature and heating capacity of this system are within 2.6% and 6.5% errors, which exhibit reasonable agreement with the experimental data.

(4) Under the indoor air temperature of test room remains at 18.0 $^{o}$C, it is recommended that the RFHC system operates at the condensing temperature of 38.0 $^{o}$C and the refrigerant mass flow rate of 3.8 kg· $h^{-1}$. Besides, it is advisable to set the copper pipe spacing with 0.25 m and the length of copper pipe with 12.0 m.

**Acknowledgements**

This work was supported by the National Key R&D Program of China (No. 2020YFD1100305-02).

**References**

[1] S. Bordignon, G. Emmi, A. Zarrella, M. De Carli, Energy analysis of different configurations for a reversible ground source heat pump using a new flexible TRNSYS Type, Applied Thermal Engineering, 197 (2021) 117413. https://doi.org/10.1016/j.applthermaleng.2021.117413

[2] L. Yang, H.Y. Yan, J.C. Lam, Thermal comfort and building energy consumption implications

Journal Pre-proofs

– A review, Applied Energy, 115 (2014) 164-173. https://doi.org/10.1016/j.apenergy.2013.10.062

[3] M.G. Zhou, T.T. Hu, Analysis of carbon emission status under the carbon neutral target in China for Earth's atmospheric balance, in: IOP Conference Series: Earth and Environmental Science, IOP Publishing, 2021, pp. 042082. https://doi.org/10.1088/1755-1315/804/4/042082

[4] Z. Li, X. Huang, Simulation analysis on operation performance of a hybrid heat pump system integrating photovoltaic/thermal and air source, Applied Thermal Engineering, 200 (2022) 117693. https://doi.org/10.1016/j.applthermaleng.2021.117693

[5] C. Su, H. Madani, B. Palm, Heating solutions for residential buildings in China: Current status and future outlook, Energy Conversion and Management, 177 (2018) 493-510. https://doi.org/10.1016/j.enconman.2018.10.005

[6] T.T. Jiang, S.J. You, Z.X. Wu, H. Zhang, Y.R. Wang, S. Wei, Performance analysis of the refrigerant-cooling radiant terminal: A numerical simulation, Applied Thermal Engineering, (197) 2021 117395. https://doi.org/10.1016/j.applthermaleng.2021.117395

[7] P.O. Fanger, N.K. Christensen, Perception of draught in ventilated spaces, Ergonomics, 29 (2) (1986) 215-235. https://doi.org/10.1080/00140138608968261

[8] S. Gendelis, A. Jakovičs, J. Ratnieks, Thermal comfort condition assessment in test buildings with different heating/cooling systems and wall envelopes, Energy Procedia, 132 (2017) 153-158. https://doi.org/10.1016/j.egypro.2017.09.668

[9] S.L. Shao, H. Zhang, S.J. You, W.D. Zheng, L.F. Jiang, Thermal performance analysis of a new refrigerant-heated radiator coupled with air-source heat pump heating system, Applied Energy, 247 (2019) 78-88. https://doi.org/10.1016/j.apenergy.2019.04.032

[10] E. Standard, Ergonomics of the thermal environment - Analytical determination and interpretation of thermal comfort using calculation of the PMV and PPD indices and local thermal comfort criteria Ergonomics of the thermal environment - Analytical determination and int, 2006.

Journal Pre-proofs

[11] L. Jin, F. Cao, D.F. Yang, X.L. Wang, Performance investigations of an R404A air-source heat pump with an internal heat exchanger for residential heating in northern China, International Journal of Refrigeration, 67 (2016) 239-248. https://doi.org/10.1016/j.ijrefrig.2016.03.004

[12] F. Causone, F. Baldin, B.W. Olesen, S.P. Corgnati, Floor heating and cooling combined with displacement ventilation: Possibilities and limitations, Energy and Buildings, 42 (12) (2010) 2338-2352. https://doi.org/10.1016/j.enbuild.2010.08.001

[13] P. Peng, G.C. Gong, X.R. Deng, C. Liang, W.Q. Li, Field study and numerical investigation on heating performance of air carrying energy radiant air-conditioning system in an office, Energy and Buildings, 209 (2020) 109712. https://doi.org/10.1016/j.enbuild.2019.109712

[14] T.T. Jiang, S.J. You, H. Zhang, S. Wei, H.Z. Liu, Y.R. Wang, Experimental study and thermo-economic analysis of a novel radiant-convective cooling system, International Journal of Refrigeration, (2021). https://doi.org/10.1016/j.ijrefrig.2021.06.013

[15] B. Xiao, L. He, S.H. Zhang, T.T. Kong, B. Hu, R.Z. Wang, Comparison and analysis on air-to-air and air-to-water heat pump heating systems, Renewable Energy, 146 (2020) 1888-1896. https://doi.org/10.1016/j.renene.2019.08.033

[16] P.M. Congedo, C. Baglivo, S. Bonuso, D. D'Agostino, Numerical and experimental analysis of the energy performance of an air-source heat pump (ASHP) coupled with a horizontal earth-to-air heat exchanger (EAHX) in different climates, Geothermics, 87 (2020) 101845. https://doi.org/10.1016/j.geothermics.2020.101845

[17] B. Hu, R.Z. Wang, B. Xiao, L. He, W. Zhang, S.H. Zhang, Performance evaluation of different heating terminals used in air source heat pump system, International Journal of Refrigeration, 98 (2019) 274-282. https://doi.org/10.1016/j.ijrefrig.2018.10.014

[18] J.J. Wu, Experimental study of thermal comfort and economic evaluation for direct radiant floor heating system with ASHP, Zhengzhou University, 2010 (in Chinese).

Journal Pre-proofs

[19] X. Dong, Q. Tian, Z. Li, Energy and exergy analysis of solar integrated air source heat pump for radiant floor heating without water, Energy and Buildings, 142 (2017) 128-138. https://doi.org/10.1016/j.enbuild.2017.03.015

[20] T.B. Li, Study on direct condensing air source heat pump radiant floor heating system, Guangdong University of Technology, 2016 (in Chinese).

[21] X.R. Wang, L. Xia, C. Bales, X.X. Zhang, B. Copertaro, S. Pan, J.S. Wu, A systematic review of recent air source heat pump (ASHP) systems assisted by solar thermal, photovoltaic and photovoltaic/thermal sources, Renewable Energy, 146 (2020) 2472-2487. https://doi.org/10.1016/j.renene.2019.08.096

[22] M.L. Qu, T.R. Li, S.M. Deng, Y.N. Fan, Z. Li, Improving defrosting performance of cascade air source heat pump using thermal energy storage based reverse cycle defrosting method, Applied Thermal Engineering, 121 (2017) 728-736. https://doi.org/10.1016/j.applthermaleng.2017.04.146

[23] J.K. Dong, S. Li, Y. Yao, Y.Q. Jiang, Y. Tian, H. Tian, Defrosting performances of a multi-split air source heat pump with phase change thermal storage, International Journal of Refrigeration, 55 (2015) 49-59. https://doi.org/10.1016/j.ijrefrig.2015.03.018

[24] Z.B. Liu, A. Li, Q.H. Wang, Y.Y. Chi, L.F. Zhang, Experimental study on a new type of thermal storage defrosting system for frost-free household refrigerators, Applied Thermal Engineering, 118 (2017) 256-265. https://doi.org/10.1016/j.applthermaleng.2017.02.077

[25] C.X. Zheng, S.J. You, H. Zhang, Z.Q. Liu, W.D. Zheng, Z.J. Wu, M. Fan, Defrosting Performance Improvement of Air-Source Heat Pump Combined Refrigerant Direct-Condensation Radiant Floor Heating System with Phase Change Material, Energies, 13 (18) (2020) 4594. https://doi.org/10.3390/en13184594

[26] F.W. Schmidt, Numerical heat transfer, International Journal of Heat and Fluid Flow, 6 (2) (1985) 68. https://doi.org/10.1016/0142-727X(85)90036-0

Journal Pre-proofs

[27] M.M. Shah, S. MM, A new correlation for heat transfer during boiling flow through pipes, ASHRAE TRANS, 82 (1976) 66-86.

[28] M.M. Shah, A general correlation for heat transfer during film condensation inside pipes, International Journal of Heat and Mass Transfer, 22 (4) (1979) 547-556. https://doi.org/10.1016/0017-9310(79)90058-9

[29] H. Zhang, Z.W. Chen, S.J. You, J.L. Wu, Thermotechnical performance study of new type floor radiant heating system with metal heat conducting film, Acta Energiae Solaris sinica, 38 (006) (2017) 1685-1691 (in Chinese).

[30] B.W. Olesen, F. Bonnefoi, E. Michel, M.D. Carli, Heat exchange coefficient between floor surface and space by floor cooling -- Theory or a question of definition, DF Liedelt Velta, Norderstedt, 2000.

[31] JG/T 403 - 2013, Test Methods for Thermal Performance of Radiant Cooling and Heating Unit, Standards Press of China, Beijing, 2013.

[32] H. Zhang, L.F. Jiang, W.D. Zheng. S.J. You, T.T. Jiang, S.L. Shao, X.M. Zhu, Experimental study on a novel thermal storage refrigerant-heated radiator coupled with air source heat pump heating system, Building and Environment, (164) 2019 106341. https://doi.org/10.1016/j.buildenv.2019.106341

[33] S.L. Shao, H. Zhang, W.D. Zheng, S.J. You, Y.R. Wang, Numerical and experimental investigations on heat transfer performance of the refrigerant-heated radiator, Applied Thermal Engineering, 179 (2020) 115748. https://doi.org/10.1016/j.applthermaleng.2020.115748

Highlights:

1) A novel ASHP system integrated with RFHC and CPCM is proposed.
2) The RFHC system is feasible and has high energy efficiency.

Journal Pre-proofs

3) The RFHC system maintains the indoor air temperature stability during defrosting.

4) A numerical model of the RFHC is established and validated to be credible.

5) The optimal operating condition and structural scheme are obtained.

## Declaration of interests

☒ The authors declare that they have no known competing financial interests or personal relationships that could have appeared to influence the work reported in this paper.

☐The authors declare the following financial interests/personal relationships which may be considered as potential competing interests:

Credit Author Statement:

**Tingting Jiang:** Investigation, Formal analysis, Writing - Original Draft

**Chenxiao Zheng:** Methodology, Investigation, Validation, Formal analysis

**Shijun You:** Conceptualization, Resources, Supervision, Project administration

Journal Pre-proofs

**Huan Zhang:** Conceptualization, Resources, Methodology, Supervision

**Zhenjing Wu:** Methodology, Software, Investigation

**Yaran Wang:** Resources, Funding acquisition, Writing – Review & Editing,

**Shen Wei:** Writing – Review & Editing

Journal Pre-proofs